A sensitive neutron spectrometer for the National Ignition Facility

R. G. Watt, R. E. Chrien, K. A. Klare, T. J. Murphy, and D. C. Wilson
Los Alamos National Laboratory, Los Alamos, New Mexico 87545

S. Haan
Lawrence Livermore National Laboratory, Livermore, California 94550

(Presented on 20 June 20000)

We are developing a sensitive neutron spectrometer for the National Ignition Facility laser at Livermore. The spectrometer will consist of a 1020 channel single-neutron-interaction time-of-flight detector array fielded 23 m from the neutron-producing target. It will use an existing detector array together with upgraded electronics for improved time resolution. Measurements of neutron yield, ion and electron temperatures, and density-radius product are all possible under certain conditions using one-, two-, or three-step reaction processes. The locations of the most important potential sources of scattered neutron backgrounds are determined as the first step in designing collimation to reduce these backgrounds. © *2001 American Institute of Physics.* [DOI: 10.1063/1.1323242]

I. INTRODUCTION

The National Ignition Facility (NIF), under construction at Lawrence Livermore National Laboratory, is designed to deliver 1.8 MJ of laser energy to mm-scale targets. This energy is 60 times more than in the previous generation of large lasers and is predicted to be sufficient for conducting inertial confinement fusion (ICF) experiments producing fusion break-even and moderate gain. The neutron yield from a target producing 1.8 MJ of fusion energy would be 6.4×10^{17}, which is eight orders of magnitude more neutrons than have been produced by hydrodynamically equivalent targets in experiments on the Nova or Omega lasers. The neutron yields predicted for the NIF imply a much larger role for fusion product diagnostics since it will be possible to measure the target conditions using a variety of higher-order processes in addition to the main fuel yield. During the commissioning phase of the NIF when full laser energy is not available, subignition ICF experiments may be performed using surrogate targets which generate low neutron yields, such as laser-plasma interaction experiments,[1] symmetry tuning experiments,[2] and noncryogenic capsule experiments including deuterated-shell[3] and double-shell capsules.[4] Furthermore, non-ICF experiments are planned for the NIF that will require sensitive neutron diagnostics. In this paper we discuss the applications and design of a sensitive neutron spectrometer (SNS) for the NIF.

II. HARDWARE DESCRIPTION OF THE SENSITIVE NEUTRON SPECTROMETER (SNS)

The SNS will be an upgraded version of the Tion (''tee-ion'') neutron spectrometer previously used on the Nova laser.[5] The spectrometer will consist of a 1020 channel array of scintillator–photomultiplier detectors. An alcove adjacent to the NIF target hall and laser switchyard #1 has been constructed to place the SNS approximately 23 m from chamber center.[6] Figure 1 shows the location of the alcove in relation to the target chamber and line-of-sight hole in the target bay wall. Details of the design, construction, and calibration of the Tion diagnostic are available elsewhere.[7,8] Because the neutron emission time is short ($\leqslant 1$ ns), the spectrum can be obtained from the arrival time distribution of individual neutron interactions in the multichannel detector array. The arrival times and velocities for gamma rays and several neutron energies are shown in Table I.

The number of neutron interactions in each plastic scintillator is given by $N = Y(A/4\pi R^2)(1 - e^{-x/\lambda})$ where Y is the neutron yield, A is the detector area, R is the distance from the NIF target to the scintillator (23 m), x is the detector thickness, and λ is the neutron mean free path for elastic scattering. The mean free path increases with neutron energy as the neutron cross section for elastic scattering from protons in the scintillator decreases; the values of λ for d–d, d–t, and 30 MeV neutrons are 7.7 cm, 27.5 cm, and 58 cm, respectively. The scintillators are mounted in an interchange-

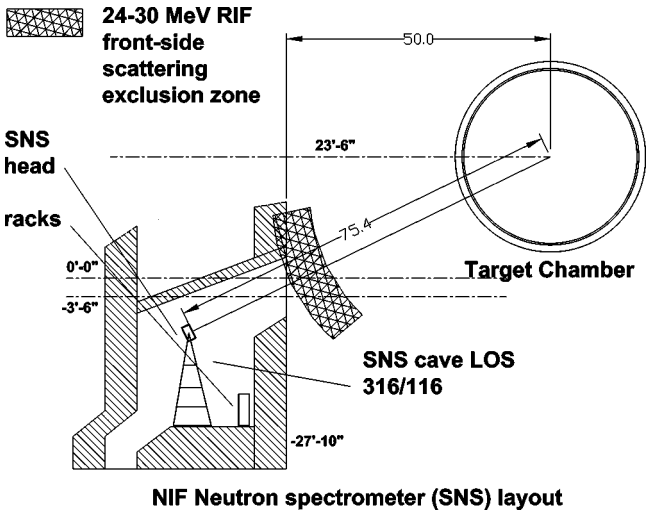

FIG. 1. Location of the SNS within the NIF target area. The shaded region indicates the location where gamma rays from inelastic scattering of primary neutrons can arrive at the detector at the same time as tertiary neutrons, for the flight path between the target and the array. Comparable scattering areas exist on the far side of the target as well, but are not shown in this figure.

TABLE I. Arrival times for a 23 m flight path on NIF.

Species	Energy (MeV)	Velocity (cm/ns)	Arrival time (ns)
Gamma rays	Any	29.98	77
Tertiary neutrons (high)	30.4	7.45	309
Tertiary neutrons (low)	20	6.90	378
Secondary neutrons (high)	17.1	5.64	408
d–t neutrons	14.05	5.14	448
Secondary neutrons (low)	11.8	4.71	489
d–d neutrons	2.45	2.16	1064

able disk; thus the neutron sensitivity can be adjusted for a particular experiment by installing a disk with the desired scintillator volume. Disks with scintillator volumes of 0.16, 0.79, or 3.53 cm^3 were used on Nova. The dynamic range available in a particular experiment can be extended by constructing a disk with multiple scintillator volumes,[9] at the cost of reducing the dynamic range in a single experiment. Lower detector sensitivity might be obtained on the NIF by constructing a disk with smaller scintillators. However, the light output from each scintillator will drop when the scintillator thickness is less than the maximum recoil proton range from the neutron elastic scattering interaction ($\simeq 2$ mm for 14 MeV recoil protons). A deuterated plastic scintillator might be used to reduce the recoil range to more accurately match the thinner scintillator used in this case. Ultimately, the neutron response of the phototubes will set the upper limit on detectable neutron yield with good timing accuracy. Each detector channel is connected to a constant fraction discriminator (CFD) with less than 0.5 ns of time walk over a 35 dB dynamic range.[10] The timing signals from the CFDs are connected to Lecroy 1877S time-to-digital converter (TDC) Fastbus modules with 0.5 ns time sampling and 20 ns conversion time. The Fastbus modules and other electronics will be controlled by a PC-based data acquisition system. The time resolution of the SNS will be determined by the neutron transit time across the scintillator (± 0.5 ns for *d–d* neutrons and 2 cm thickness), the photomultiplier tube (PMT) transit time spread (1 ns for 10 photoelectrons from a 0.25 MeV recoil proton), the time walk in the CFD (± 0.25 ns over the maximum dynamic range), and the sampling time of the TDCs (0.5 ns). These factors, combined in quadrature, suggests that a resolution of 1.3 ns can be achieved. This time resolution corresponds to an energy resolution for *d–d* neutrons of 6 keV (0.24%). For *d–t* neutrons the neutron transit time (± 0.2 ns for a 2 cm thickness) and PMT spread (0.2 ns) will be smaller, resulting in estimated time and energy resolution of 0.6 ns and 39 keV (0.28%). Better energy resolution will be obtained with thinner scintillators. The actual time resolution can be inferred from the observed width of the hard x-ray pulse produced by NIF targets.

III. APPLICATIONS OF THE SNS

A. Neutron yield

The SNS will provide the most sensitive measurement of neutron yield on the NIF. Yields of *d–d* neutrons as low as 4×10^6 can be measured with $<30\%$ statistical uncertainty. The SNS can operate as a single-interaction detector array for *d–d* neutron yields up to 3×10^9 using the existing 0.16 cm^3 scintillators or could be extended to higher yields with smaller scintillators. Other core neutron diagnostics on NIF are likely to make such an extension unnecessary.[11] The maximum yield for *d–t* and 30 MeV tertiary neutrons will be approximately 1×10^{10} and 2×10^{10}, respectively. The yield calibration will be determined through a combination of intrinsic calibration (distance, solid angle, and neutron attenuation), accelerator calibration using the associated particle technique, and cross calibration to other NIF yield diagnostics such as neutron activation. These neutron yields can be used for determining the fusion reactivity in laser-plasma interaction experiments with gas-filled hohlraums containing deuterated neopentane,[12] $Xe–D_2$,[1] or He–H gas fills with trace quantities of deuterium. Another application is measuring the yield from a deuterated layer[3] in the ablator of an ICF capsule filled with nonreacting hydrogen gas for comparison with simulations of the thermal conduction losses from the compressed core into the ablator. The depth of the deuterated layer can be varied in separate capsules to map out the temperature profile in the ablator.

B. Ion temperature from primary neutrons

In ICF targets where the bulk fluid speed is negligible compared with the ion thermal speed,[12] the neutron energy spectrum may be used to diagnose the temperature of the fuel.[13] When the target yield is less than $1-2\times10^9$, the spectra from conventional current-mode TOF detectors suffer from statistical fluctuations in the rate of neutron interactions in the detector and the quantity of scintillation light created in each interaction.[14] For these targets, single-neutron-interaction detector arrays[7,15,16] are used to increase sensitivity by measuring the arrival times of individual neutrons and constructing a spectrum from many detector channels. Results from current-mode detectors and single-interaction arrays on the Nova laser indicate that their useful ranges of neutron yield overlap by less than a factor of 2.[8] The SNS can determine T_i for *d–d* neutron yields in the range from 2×10^7 to 3×10^9 and for *d–t* neutron yields in the range from 6×10^7 to 1×10^{10}. The ion temperature is determined from the spread in neutron energy by the relation from Brysk[13] $\Delta E_n(\mathrm{keV}) = C_{dt}\sqrt{T_i(\mathrm{keV})}$ where ΔE_n is the energy spread (FWHM) and $C_{dt}=176$ (for *d–d* reactions the coefficient is $C_{dd}=82.5$). The energy spectrum is related to the arrival time spectrum by the relativistic time-of-flight relation $E=(m/2)(R/t)^2/\sqrt{1-(R/ct)^2}$ where t is the arrival time. The energy spectrum must be corrected for the instrumental time resolution applicable to the primary neutron peak involved. This correction is equivalent to subtracting the ''temperature'' corresponding to the instrumental energy resolution through the Brysk relation.

C. Measurements using secondary neutrons

In small or weakly compressed ICF capsules filled with deuterium gas, the average density-radius product (ρR) of the fuel region can be determined by measurements of the secondary (*d–t*) neutrons.[17] The *d–d* fusion reaction has two

TABLE II. Combinations of distance from the target and angle from the SNS flight path at which a primary *d–t* neutron could create a gamma ray through inelastic scattering that has the same arrival time at the SNS as a tertiary neutron.

Angle (degrees)	30.4 MeV tertiary distance (m)	28 MeV tertiary distance (m)	26 MeV tertiary distance (m)	24 MeV tertiary distance (m)
0	14.4	15.2	15.9	16.7
10	14.3	15.0	15.7	16.5
20	14.0	14.7	15.4	16.1
30	13.6	14.3	14.9	15.7
45	13.0	13.7	14.3	15.0

branches, $d(d,n)^3He$ and $d(d,p)t$, with nearly equal branching ratios. The tritons in the second branch, which are born with 1.01 MeV of energy, can undergo reactions in flight with the deuterium fuel and produce secondary *d–t* neutrons by this two-step process. The ratio of the secondary to primary neutron yield thus provides a measurement of the triton burnup.

1. Low ρR

For capsules with low values of ρR ($<0.01\,g/cm^2$) the triton loses little energy as it escapes from the fuel region. The secondary $d(t,n)^4He$ reactions occur at the cross section corresponding to the triton birth energy and the triton burnup is proportional to ρR. The SNS will be able to measure the secondary neutron spectrum from low-ρR capsules ($\rho R = 0.001\,g/cm^2$) for primary *d–d* neutron yields as high as 4×10^{14} as in exploding pusher capsules.

2. Moderate ρR

For larger values of ρR ($0.01\,g/cm^2 < \rho R < 0.10-0.50\,g/cm^2$, depending on T_e), the tritons escape but have significant energy loss within the fuel region. The triton burnup increases as its energy approaches the peak of the $d(t,n)^4He$ cross section at $\simeq$170 keV. In this case the burnup is not uniquely dependent on ρR but also depends on T_e (through its effect on the time that the triton spends near the peak of the cross section) and n_d/n_e (as a result of fuel dilution due to mix). The triton burnup can vary from 1×10^{-3} to 1×10^{-1} in this regime. Depending on the value of the triton burnup, the SNS will be able to record the secondary neutron spectrum for primary *d–d* neutron yields as high as 4×10^{13}. It has been shown[18] that the secondary neutron spectrum is uniquely related to the energy spectrum of the tritons responsible for the secondary reactions. The ρR can be determined from the reacting triton spectrum through a model for the triton energy loss. When the ρR is low, the reacting tritons are peaked at their 1 MeV birth energy and produce a rectangular secondary neutron spectrum extending from 11.8 to 17.1 MeV. When the ρR is high, the reacting tritons are peaked near the maximum of the cross section and produce a secondary neutron spectrum with a full width at half maximum (FWHM) of $\simeq$2 MeV.

3. High ρR

For large values of ρR ($>0.50\,g/cm^2$) all the tritons thermalize within the fuel. The triton burnup has no dependence on ρR, but varies as $T_e^{3/2}$ for low T_e and reaches $\simeq$50% burnup at 10 keV. The burnup also scales linearly with n_d/n_e. It may provide a useful lower bound for T_e (assuming no mix) or a measurement of n_d/n_e if T_e is determined by another diagnostic. Depending on the burnup, the SNS should be able to measure the secondary neutron spectrum for primary *d–d* neutron yields as high as 2×10^{12}.

D. ρR measurements using tertiary neutrons

The ρR of ICF capsules approaching ignition conditions can be determined by measuring the high-energy ''tertiary'' neutrons produced in a three-step process.[19] The steps are

(1) A primary *d–t* reaction produces a 14 MeV neutron.
(2) The neutron has an elastic scattering reaction with a fuel deuteron (or triton), boosting its energy as high as 12.5 MeV (10.5 MeV for a triton).
(3) The scattered deuteron (or triton) fuses with a fuel triton (or deuteron), producing a tertiary neutron with energy as high as 30 MeV.

Both the neutron produced in step 1 and the highest-energy deuterons produced in step 2 have ranges which are longer than the size of the ''hot spot'' in the fuel region in NIF capsules and lose little energy in this region. As a result, the probabilities of steps 2 and 3 each scale with ρR and the ratio of tertiary to primary neutrons scales as $(\rho R)^2$. The constant of proportionality depends on the energy range of the tertiary neutrons detected, and is approximately 1×10^{-5} (ρR in g/cm^2) for tertiary neutrons between 24 and 30 MeV. Significant energy loss may occur for elastically scattered deuterons (or tritons) with much less than the maximum recoil energy, especially for the ρR values expected for ignition and high-yield capsules. Interpretation of the complete tertiary neutron spectrum will require detailed capsule simulations and will involve assumptions about the correct charged particle energy loss model to use in the simulations. The SNS should be able to measure the leading edge of the tertiary neutron arrivals (for which uncertainties in the slowing-down model are minimized) from near-ignition capsules ($\rho R \simeq 0.2\,g/cm^2$) with primary neutron yields up to 5×10^{16}. This yield is within an order of magnitude of capsule breakeven and thus the SNS should be useful for ρR measurements in most preignition targets. Only the highest energy part of the tertiary neutron spectrum will be recorded

since the detector array will see a rapidly increasing neutron flux after each channel has detected its first neutron arrival.

IV. NEUTRON SCATTERING AND BACKGROUNDS

The tertiary neutrons are expected to be a weak signal in early NIF experiments so minimizing the competing background signals will be important. The shaded region in Fig. 1 indicates locations where (n,γ) reactions caused by primary d–t neutrons can create a background for tertiary neutron arrivals in the flight path between the target and the array. Comparable scattering centers exist on the far side of the chamber as well but are not shown in the figure to allow a blown up view of the region in the direct flight path. In these locations the combined flight time of a primary neutron and the gamma ray it creates through inelastic scattering can equal the flight time of a tertiary neutron. For cryogenic d–t-filled capsules reaching ignition-relevant ρR values, the SNS will saturate on the leading edge of the tertiary neutron arrivals (24–30 MeV). For this range of tertiary neutron energies, the background created by primary neutrons traveling close to the SNS flight path is created in materials located 14–17 m from the target. Therefore scattering materials must be excluded from this region. Primary neutrons traveling at larger angles to the SNS flight path and which scatter from materials at shorter distances from the target could also contribute to the background (Table II), but their effect can be eliminated by installing a collimator near the entrance to the SNS alcove. We plan to design this collimator and simulate the NIF scattering environment using the MCNP code.[20] Scattering within the SNS detector housing creates a tail on the primary d–t neutron spectrum and complicates the determination of ion temperature.[8] We plan to use the MCNP code to evaluate modifications to the detector hardware that could reduce the close-in scattering. By locating the SNS on an elevated platform, we can keep nearby sources of scattered neutron backgrounds to a minimum.

ACKNOWLEDGMENT

Work supported by US DOE Contract No. W-7405-ENG-36.

[1] J. C. Fernández *et al.*, Phys. Rev. Lett. **77**, 2702 (1996).
[2] N. D. Delamater *et al.*, Phys. Plasmas **7**, 1609 (2000).
[3] R. E. Chrien *et al.*, Phys. Plasmas **5**, 768 (1998).
[4] W. S. Varnum *et al.*, Phys. Rev. Lett. **84**, 5153 (2000).
[5] R. E. Chrien, K. A. Klare, and T. J. Murphy, Rev. Sci. Instrum. **68**, 607 (1997).
[6] D. Lee (private communication).
[7] R. E. Chrien, D. F. Simmons, and D. L. Holmberg, Rev. Sci. Instrum. **63**, 4886 (1992).
[8] R. E. Chrien *et al.*, Fusion Eng. Des. **34–35**, 557 (1997).
[9] M. Cable (private communication).
[10] C. Thompson (private communication).
[11] T. J. Murphy *et al.*, Rev. Sci. Instrum. (these proceedings).
[12] T. J. Murphy, R. E. Chrien, and K. A. Klare, Rev. Sci. Instrum. **68**, 614 (1997).
[13] H. Brysk, Plasma Phys. **15**, 611 (1973).
[14] R. A. Lerche and B. A. Remington, Rev. Sci. Instrum. **61**, 3131 (1990).
[15] M. D. Cable, J. Appl. Phys. **60**, 3068 (1986).
[16] M. B. Nelson and M. D. Cable, Rev. Sci. Instrum. **63**, 4874 (1992).
[17] T. E. Blue and D. B. Harris, Nucl. Sci. Eng. **77**, 463 (1981).
[18] M. D. Cable and S. P. Hatchett, J. Appl. Phys. **62**, 2233 (1987).
[19] H. Azechi, M. D. Cable, and R. O. Stapf, Laser Part. Beams **9**, 119 (1991).
[20] J. F. Briesmeister, Los Alamos National Laboratory Report No. LA-12625-M, 1993.